Viscometric Studies of Poly(*N*-vinyl-2-pyrrolidone) in Water and in Water and 0.01% Bovine Serum Albumin at 283.15, 288.15, 293.15, 298.15, 303.15, 308.15, and 313.15 K

Man Singh, Sanjay Kumar

Chemistry Research Laboratory, Deshbandhu College, University of Delhi, New Delhi, 110019, India

Received 15 June 2001; accepted 17 April 2002

ABSTRACT: Viscosity and density studies for 0.01–0.14% (w/w) poly(*N*-vinyl-2-pyrrolidone) (PVP) in water and in water and 0.01% bovine serum albumin (BSA) were conducted at 283.15, 288.15, 293.15, 298.15, 303.15, 308.15, and 313.15 K. The viscosity coefficients and the activation-energy, free-energy, enthalpy, and entropy changes were calculated from viscosity data for viscous flow. On this basis, PVP–PVP, PVP–BSA, PVP–water, and BSA–water interactions and PVP and BSA shape factors were investigated and rationalized in terms of the water structure. © 2002 Wiley Periodicals, Inc. J Appl Polym Sci 87: 1001–1015, 2003

Key words: bovine serum albumin; viscosity coefficient; enthalpy changes; shape factor

INTRODUCTION

The viscometric behavior of a polymer in a solution of second polymer[1–5] with a constant concentration has proven to be useful for investigating changes in polymer dimensions in solution. Work on poly(*N*-vinyl-2-pyrrolidone) (PVP) is currently of interest in the field of polymer science and in other allied areas.[6] In this study, we focused on measuring the densities, viscosities, activation-energy changes (ΔE^*), free-energy changes (ΔG), enthalpy changes (ΔH), and entropy changes (ΔS) for viscous flow for PVP in water and in water and 0.01% bovine serum albumin (BSA) as functions of the PVP concentration and temperature for a complete understanding of the integrated protein interactions because such studies had not been carried out on these systems previously. Therefore, the studies were designed to provide data on PVP in water and in water and 0.01% BSA from 283.15 to 313.15 K.

EXPERIMENTAL

PVP (molecular weight = 40,000; BDH, India) and BSA (molecular weight = 65,000; Sigma) were used as received. The solutions for PVP and BSA were prepared by weight percentage in triple-distilled, demineralized, and degassed water. A double-limb pycnometer and an Ubbelohde viscometer were used to measure the densities and viscosities, respectively. The temperature was controlled with an autoelectric relay circuited to a contact thermometer, which included a 25-W immersion rod. A low temperature was obtained with an MK-70 water cooling machine (New Delhi, India). The cold water from the machine's reservoir was circulated through thick-walled PVC pipes joined by the circulating ends of a TULLU pump (UP National MFRS Ltd., Varansi, India) and by a copper coil fixed between the PVC pipes. The temperature was controlled to ± 0.01°C and was repeatedly checked with a Beckmann thermometer (Labortherm-N Skalenwert 0.01 K made in GDR) calibrated by the National Physical Laboratory (New Delhi, India). The efflux time for viscosity measurements was noted with a digital electronic racer watch with an accuracy of 1.0×10^{-2} s.

Density and viscosity measurements

The solution densities were calculated as follows:

$$\rho = \frac{M_{\text{soln}}}{M_{\text{slv}}}\rho_{\text{water}} + \rho_{\text{air}}\left(1 + \frac{M_{\text{soln}}}{M_{\text{solv}}}\right) \quad (1)$$

where ρ is the solution density; ρ_{water} and ρ_{air} are the densities of water and air, respectively; and M_{soln} and M_{solv} are the masses of the solution and solvent, respectively. The second term in eq. (1) is used for the buoyancy correction of air. ρ_{air} and ρ_{water} values were taken from the literature. The measurements were carried out at 780 mmHg, as measured by a barometer in the laboratory.

Correspondence to: M. Singh (mansingh50@hotmail.com).

Journal of Applied Polymer Science, Vol. 87, 1001–1015 (2003)

TABLE I
Comparison of Experimental Dynamic Viscosities (η_{exp}'s) and Literature Dynamic Viscosities (η_{lit}) for Water

Temperature (K)	283.15	288.15	293.15	298.15	303.15	308.15	313.15
η_{exp} (cP)	1.3155	1.1344	1.0139	0.8834	0.7996	0.7314	0.6623
η_{lit}[a] (cP)	1.3037	1.1369	1.0019	0.8909	0.7982	—	0.6540
Δ	0.0118	−0.0025	0.0120	−0.0075	0.0014	—	0.0083

$\Delta = \eta_{exp} - \eta_{lit}$.
[a] Ref. 18.

TABLE II
ρ Constants for PVP in Water, BSA in Water, and PVP in 0.01% BSA and Water Obtained by Regression Analysis of the Equation $\rho = \rho^0 + ac + bc^2$

Temperature	PVP in water			BSA in water			PVP in 0.01% BSA and water		
ln K	ρ^0	a	b	ρ^0	a	b	ρ^0	a	b
283.15	1.0021	0.0335	−0.2016	1.0023	0.0158	−0.1639	1.0021	0.0052	—
288.15	1.0007	0.0313	−0.1594	1.0015	0.0190	−0.1889	1.0017	−0.0011	—
293.15	0.9998	0.0324	−0.1621	0.9997	0.0205	−0.0250	1.0004	0.0050	—
298.15	0.9996	0.0016	—	0.9987	0.0184	—	0.9991	0.0017	—
303.15	0.9974	0.0180	−0.0906	0.9972	0.0176	−0.0889	0.9978	0.0001	—
308.15	0.9960	0.0223	−0.0919	0.9967	0.0134	−0.1278	0.9969	−0.0025	—
313.15	0.9940	0.0299	−0.1457	0.9953	−0.0034	—	0.9954	−0.0088	—

TABLE III
ρ Constants for PVP in Water, BSA in Water, and PVP in 0.01% BSA and Water Obtained by Regression Analysis of the Equation $\rho = \rho^0 + aT$

	PVP in water		BSA in water		PVP in 0.01% BSA and water	
c (wt %)	ρ^0	a	ρ^0	a	ρ^0	a
0.01	1.0750	−0.0003	1.0715	−0.0002	1.0708	−0.0002
0.04	1.0800	−0.0003	1.0728	−0.0002	1.0649	−0.0002
0.07	—		1.0759	−0.0003	1.0849	−0.0003
0.10	1.0757	−0.0003	1.0734	−0.0002	1.0747	−0.0003
0.14	1.0738	−0.0002	—	—	—	—

TABLE IV
Constants of η Obtained by Least Square Fitted to the Equation $\eta - \eta^0 + ac$

Temperature	PVP in water		BSA in water		PVP in 0.01% BA and water	
(K)	η^0 (cP)	a	η^0 (cP)	a	η^0 (cP)	a
283.15	1.3198	0.2646	1.3195	0.1534	1.3235	0.2676
288.15	1.1527	0.1392	1.1549	0.0501	1.1511	0.2592
293.15	1.0067	0.2185	1.0087	0.1568	1.0102	0.3174
298.15	0.8956	0.1938	0.8975	0.1032	0.8987	0.2614
303.15	0.7991	0.1968	0.8036	0.1275	0.8075	0.1731
308.15	0.7263	0.1513	0.7322	0.0687	0.7355	0.1018
313.15	0.6674	0.0709	0.6679	0.0150	0.6659	0.1665

TABLE V
Constants of η Obtained by Least Square Fitted to the Equation $\eta = \eta^0 + aT$

	PVP in water		BSA in water		PVP in 0.01% BSA and water	
c (wt %)	η^0 (cP)	a	η^0 (cP)	a	η^0 (cP)	a
0.01	7.3823	−0.0216	7.3846	−0.0216	7.3984	−0.0216
0.04	7.4108	−0.0217	7.3107	−0.0214	7.3403	−0.0214
0.07		—	7.4447	−0.0218	7.5274	−0.0220
0.10	7.5189	−0.0220	7.4363	−0.0218	7.5204	−0.0220
0.14	7.5547	−0.0221				

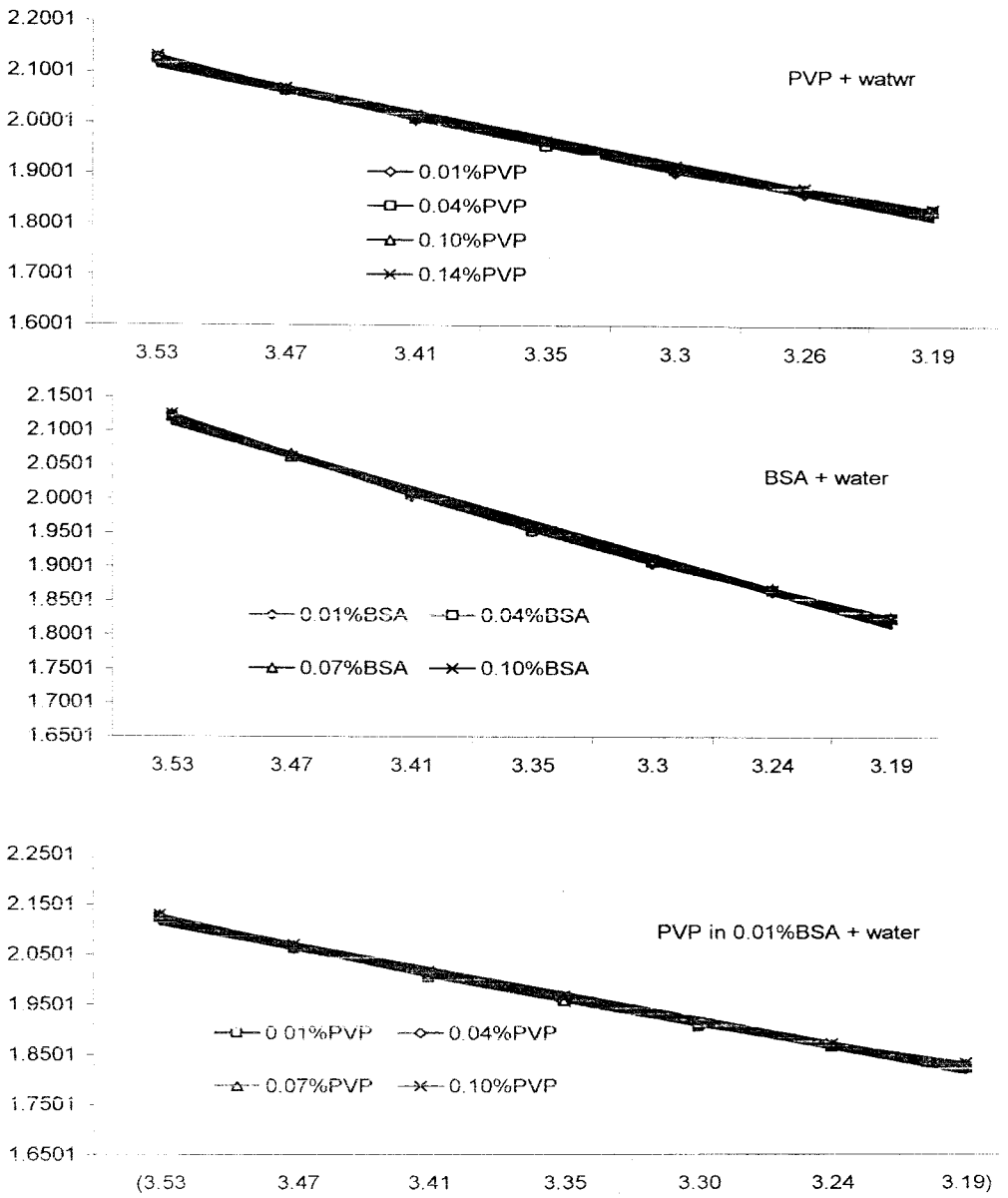

Figure 1 Log $\eta + 2$ (y axis) versus $1/T \times 10^3$ (x axis).

The dynamic viscosity (η) of the solutions was calculated as follows:

$$\eta = \left(At - \frac{V}{8\pi lt}\right)\rho \tag{2}$$

where A is a viscometer calibration constant, $V/8\pi l$ is a kinematic energy correction term, V is the flow volume, l is the capillary length, and t is the efflux time. The viscometer was calibrated with deionized, triple-distilled, degassed water and toluene. The experiments were repeated 10 times with water and toluene at each temperature under similar conditions. Our method was standardized with known viscosity values of water; as shown in Table I, the experimental values closely agreed with literature values.

The reduced viscosity (η_{red}) obtained from η was best-fit against c as follows:

$$\eta_{red} = \frac{\eta/\eta^0 - 1}{c} = B + Dc + D'c^2 \tag{3}$$

where η^0 is the dynamic viscosity of the solvent, c is the concentration, B is the intercept, and D and D' are the slope constants.

The activation energy (E^*) for viscous flow was evaluated by the plotting of log η versus $1/T$ (Fig. 1). The slope of this plot was used to calculate E^*:

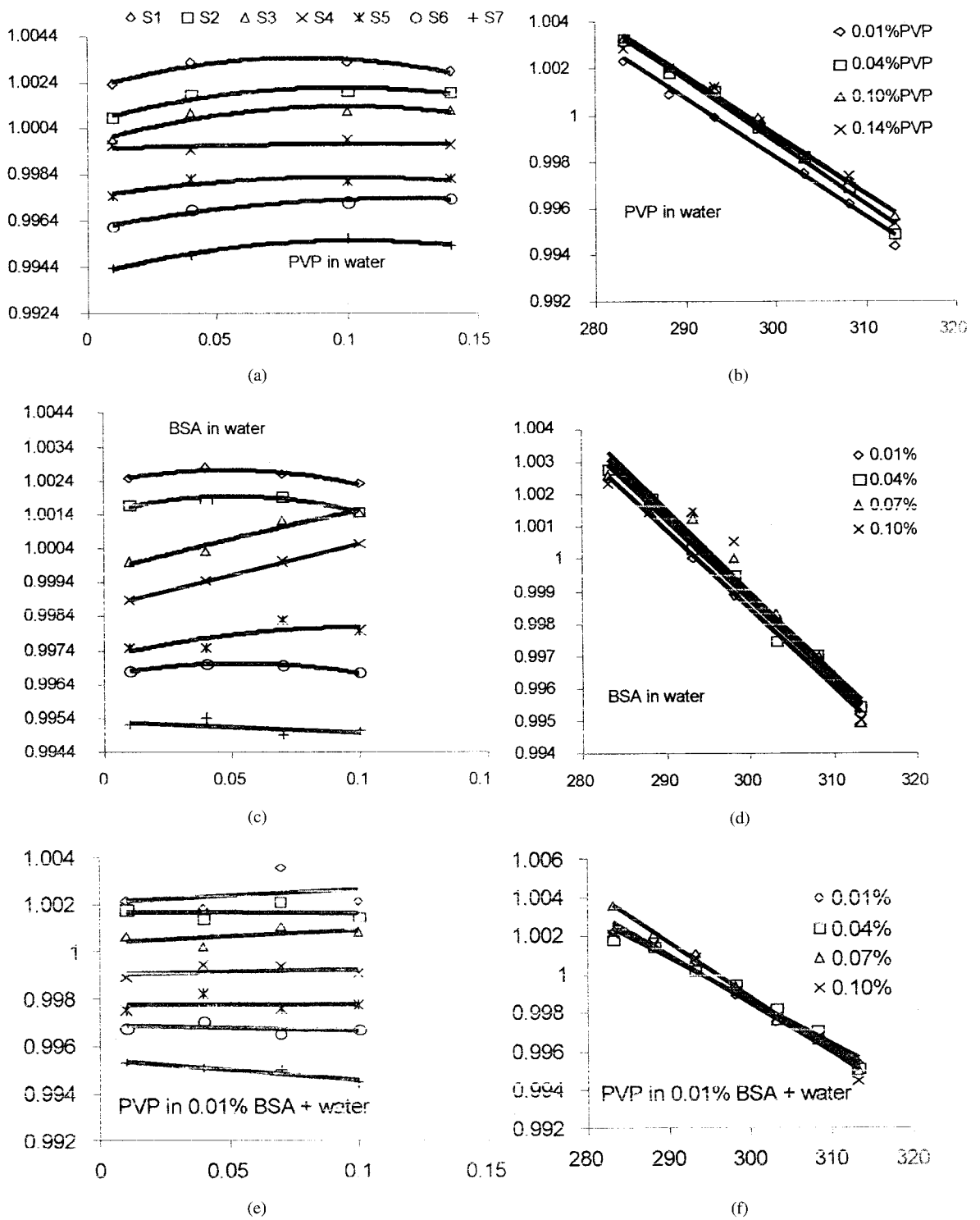

Figure 2 ρ (g/cc; y axis) versus the concentration of the solute (wt %; x axis) on the left (S1 = 283.15, S2 = 288.15, S3 = 293.15, S4 = 298.15, S5 = 303.15, S6 = 308.15, and S7 = 313.15 K) and versus the temperature (K; x axis) on the right.

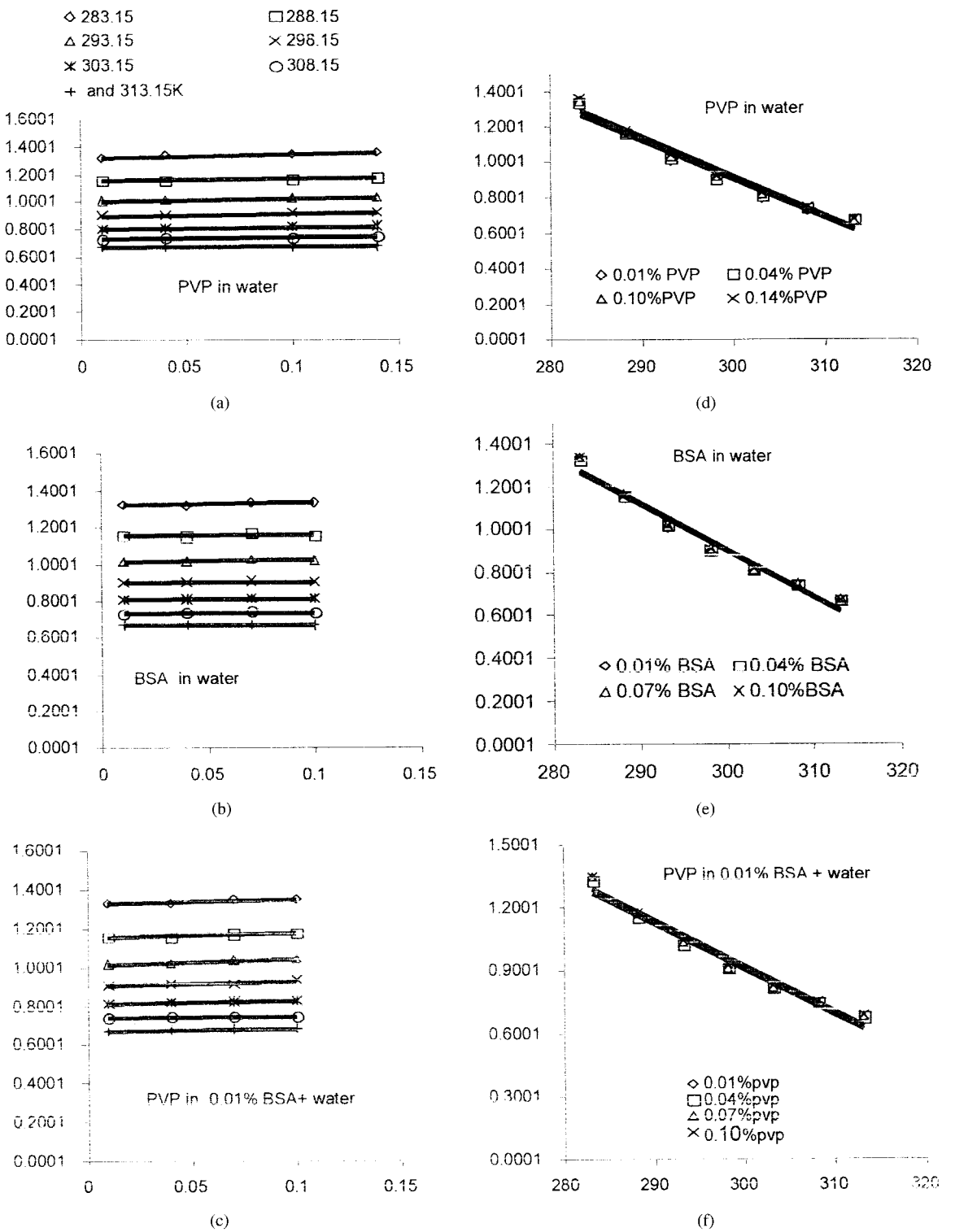

Figure 3 η (cP; y axis) versus the concentration of the solute (wt %; x axis) on the left and versus the temperature (K; x axis) on the right.

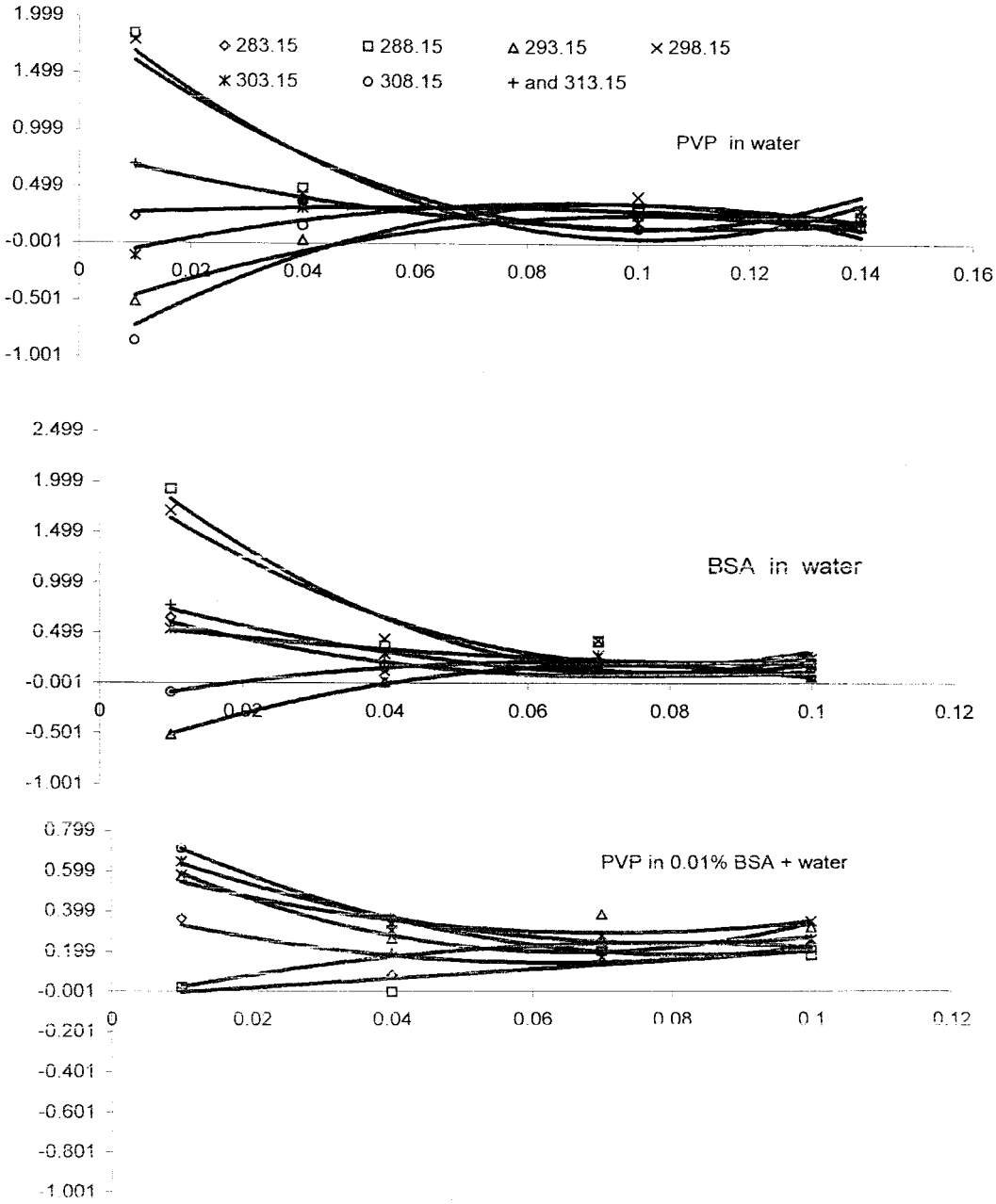

Figure 4 η_{red} (cm^3/g; y axis) versus the concentration of the solute (wt %; x axis).

TABLE VI
Regression Constants for η_{red} Obtained by Best Fitting to the Equation $\eta_{red} = B + Dc + D'c^2$

Temperature (K)	PVP in water			BSA in water			PVP in 0.01% BSA and water		
	B	*D*	*D'*	*B*	*D*	*D'*	*B*	*D*	*D'*
283.15	0.25	2.35	−19.53	0.79	−20.18	141.82	0.41	−8.31	65.02
288.15	2.10	−40.17	198.60	2.37	−57.86	369.82	−0.03	2.30	−0.10
293.15	−0.63	17.25	−85.02	−0.74	25.23	−171.96	0.63	−9.70	68.53
298.15	1.96	−36.54	182.35	2.09	−47.85	301.68	0.74	−16.58	125.89
303.15	−0.16	11.71	−65.67	0.60	−8.40	43.92	0.76	−12.95	80.73
308.15	−1.00	28.35	−148.55	−0.22	13.48	−107.29	0.87	−16.59	100.47
313.15	0.80	−11.90	53.387	0.92	−19.95	118.78	−0.05	7.41	−47.30

TABLE VII
ΔG, ΔH, and ΔS for PVP in Water and 0.01% BSA Water at 283.15 K

	In water				0.01% BSA and water		
C (wt %)	$n \times 10^{-7}$	$-\Delta G \times 10^{-7}$	$\Delta H \times 10^{-2}$	$\Delta S \times 10^{-4}$	$-\Delta G \times 10^{-7}$	$\Delta H \times 10^{-2}$	$\Delta S \times 10^{-4}$
0.01	2.5	13.85	12.65	4.47	21.30	12.57	4.44
0.04	10	355.29	50.30	17.76	76.35	50.27	17.75
0.07	17.5	—	—	—	688.25	87.38	30.86
0.10	25	1349.23	125.24	44.24	1127.33	124.68	44.04
0.14	35	2486.79	174.70	61.71			
288.15							
0.01	2.5	109.36	15.08	5.23	1.04	14.93	5.18
0.04	10	462.33	60.27	20.92	−4.14	59.72	20.73
0.07	17.5				583.48	103.78	36.02
0.10	25	1702.41	149.99	52.06	1057.94	147.97	51.36
0.14	35	2756.21	209.52	72.72			
293.15							
0.01	2.5	−31.33	17.66	6.03	34.94	17.66	6.02
0.04	10	26.43	70.45	24.03	254.84	70.47	24.04
0.07	17.5				1131.03	122.33	41.73
0.10	25	1001.56	174.76	59.62	1909.24	174.34	59.48
0.14	35	1848.05	244.01	83.24			
298.15							
0.01	2.5	109.88	20.73	6.95	35.77	20.51	6.88
0.04	10	434.01	82.94	27.82	298.97	81.77	27.43
0.07	17.5				518.43	143.11	48.00
0.10	25	2529.77	204.93	68.74	2129.19	202.15	67.81
0.14	35	3532.25	286.92	96.25			
303.15							
0.01	2.5	−7.10	23.91	7.88	40.63	23.69	7.81
0.04	10	316.44	94.97	31.33	339.52	94.42	31.15
0.07	17.5				847.90	164.76	54.35
0.10	25	1580.06	235.94	77.83	1617.58	234.61	77.39
0.14	35	2780.61	329.25	108.62			
308.15							
0.01	2.5	−55.42	27.11	8.79	45.43	26.92	8.74
0.04	10	160.66	107.62	34.93	369.07	107.29	34.82
0.07	17.5				621.66	187.80	60.95
0.10	25	869.97	268.07	86.99	1344.74	267.33	86.76
0.14	35	1856.83	373.96	121.36			
313.15							
0.01	2.5	15.06	30.67	9.79	0.97	30.54	9.75
0.04	10	394.13	122.19	39.02	198.24	121.72	38.87
0.07	17.5				697.94	212.19	67.76
0.10	25	1033.71	305.37	97.52	1456.55	302.05	96.46
0.14	35	2121.94	425.93	136.02			

$$E^* = \text{Slope} - 2.303\,\text{R} \tag{4}$$

where R is the gas constant (8.3144 J mol^{-1} K^{-1}). ΔG, ΔS, and ΔH were calculated with the following modified equations, and the values are reported later in Table VII:

$$\Delta G = -2.303nRT \log \frac{\eta}{\eta^0} \tag{5}$$

$\Delta\eta$ is taken as the difference of the solution and solvent viscosities:

$$\Delta S = -\left(\frac{\Delta G}{\Delta \eta}\right)_{\text{PT}} \tag{6}$$

$$\Delta H = \Delta G + T\Delta S \tag{7}$$

RESULTS AND DISCUSSION

The ρ and η trends for PVP in water and in water and 0.01% BSA as a PVP concentration function at various temperatures are shown in Figures 2 and 3. The PVP density trend remains polynomial at 283.15, 288.15, and 293.15 K [Fig. 2(a)], but at 298.15 K, it becomes linear with the PVP concentration. Again, after 298.15, the polynomial trend is regained for 303.15, 308.15, and 313.15 K [Fig. 2(a)]. Regression constants for density are given in Table II. For similar systems, the density decreases as the temperature rises [Fig. 2(b)]. However, with the addition of PVP to water and BSA, the density changes linearly at chosen temperatures

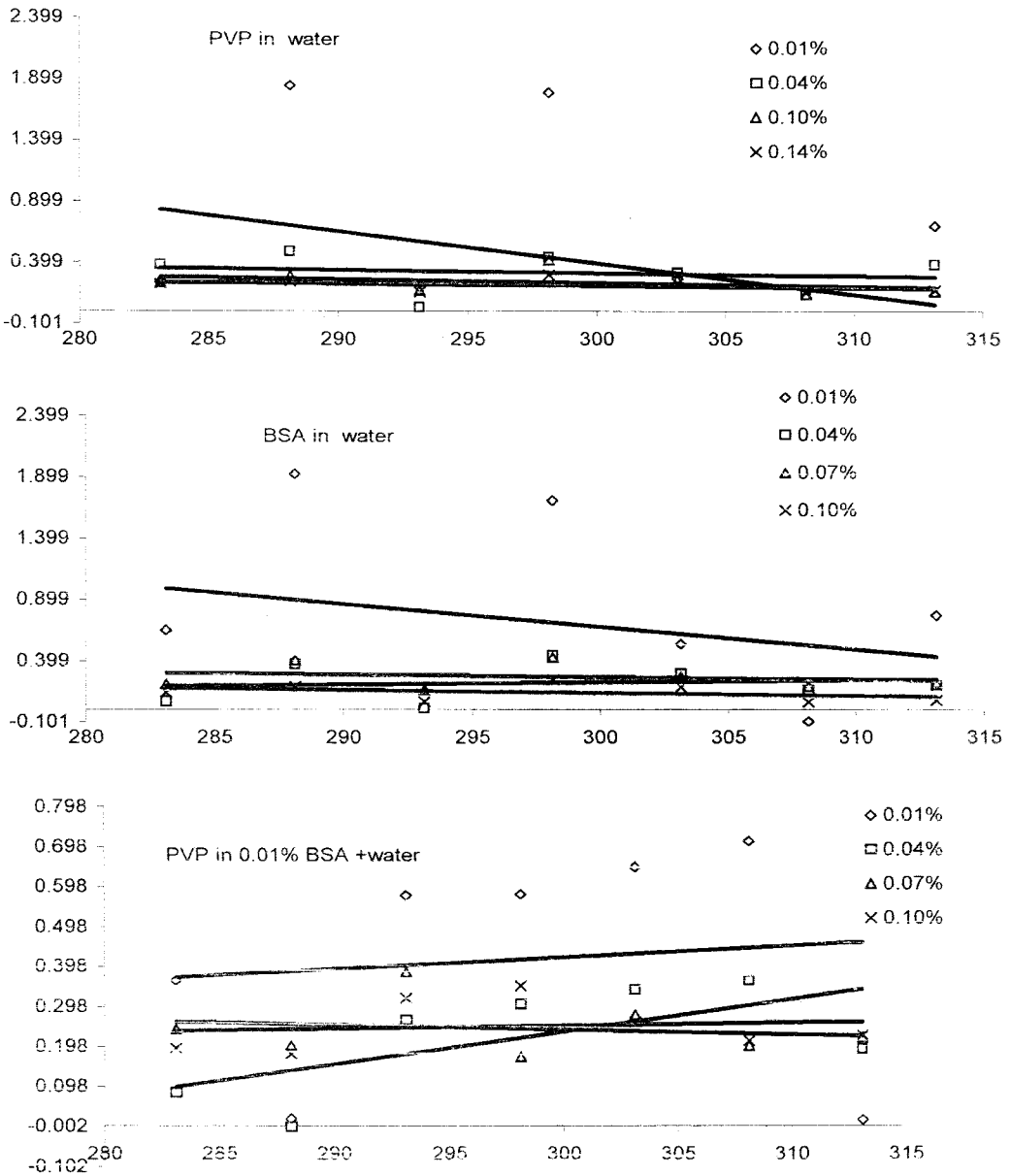

Figure 5 η_{red} (cm^3/g; y axis) versus the temperature (K; x axis) for various concentrations of the solute.

with a positive slope, except for 288.15, 308.15, and 313.15 K [Fig. 2(e)]. The density for BSA in water is linear at 293.15, 298.15, and 313.15 K, whereas at other chosen temperatures, it is polynomial [Fig. 2(c)]; the slope at 313.15 K is negative.

The densities for PVP and BSA in water and for PVP in water and BSA decrease with temperature, but at similar temperatures, they increase as the PVP and BSA concentrations rise and as the PVP in water and BSA concentrations rise [Fig. 2(b,d,f)] with a negative slope (Table III). The limiting densities for PVP and BSA in water and for PVP in water and BSA increase to 0.04–0.07%, but after 0.07%, the latter decreases (Table III).

The η trend for PVP and BSA in water and for PVP in water and BSA is linear with a positive slope at chosen temperatures (Fig. 3; because the PVP and BSA molecules are larger and integrated even in their aqueous solutions, the viscosity is taken as the function of their rotational dynamics; therefore, the measured viscosities are called dynamic viscosities). Notably, the broader viscosity–temperature bands of the spectra at lower temperatures tend to narrow with increasing temperature [Fig. 3(a–c)]. This signifies a larger change in the viscosity as the temperature is increased by 5°C at a lower temperature region, whereas a similar variation at a higher temperature leads to lower viscosity changes [Fig. 3(a–c)].

The viscosities for PVP and BSA in water and for PVP in BSA and water decrease with a negative slope as the temperature increases [Fig. 3(d–f)] (Table V).

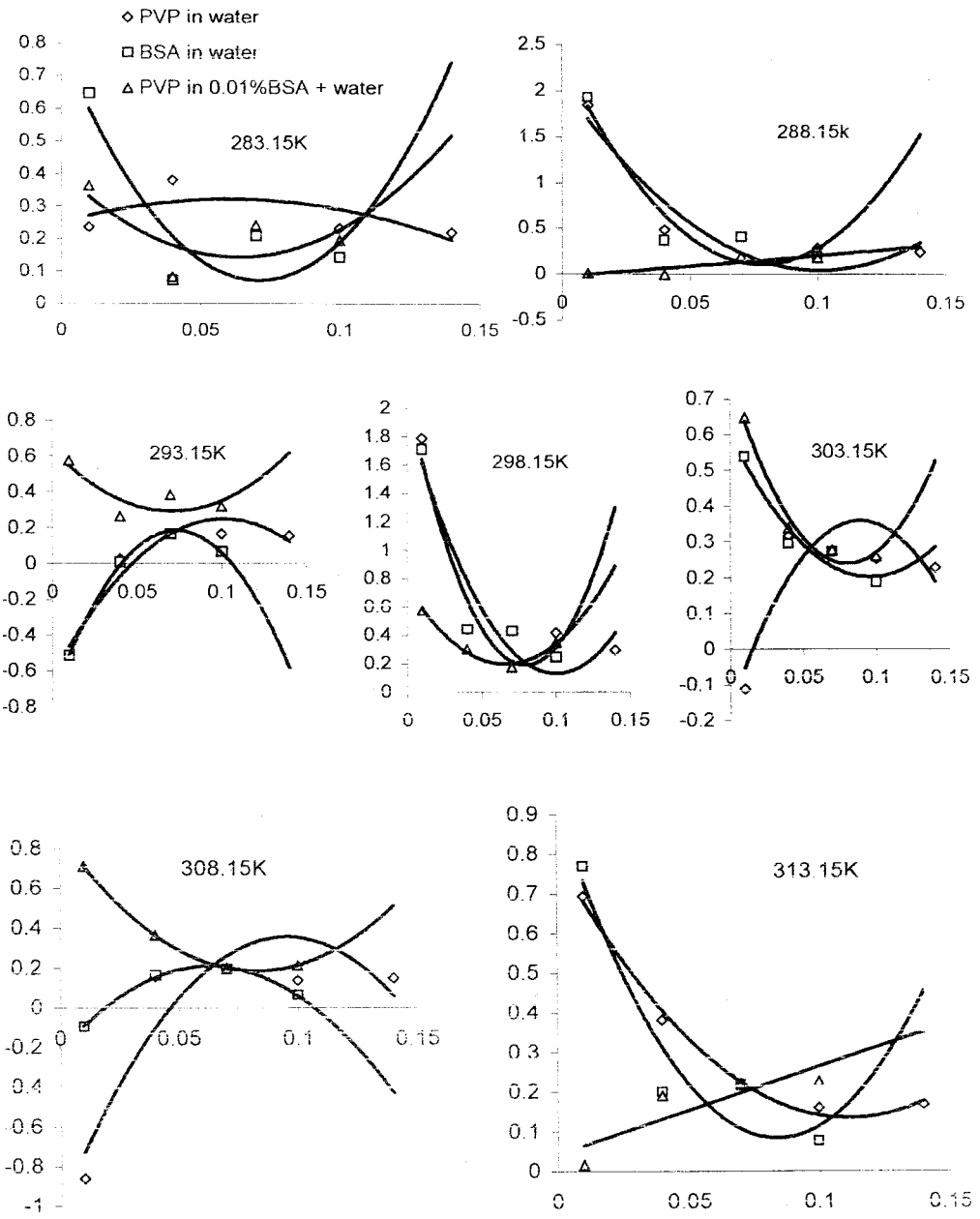

Figure 6 η_{red} (cm^3/g; y axis) versus the concentration of the solute (wt %; x axis) for various temperatures.

These trends could be attributed to the smaller structural changes of water and PVP, water and BSA, and water–PVP–BSA, as shown later in Figure 10.

As for density, there may be more interactions at low concentrations [Fig. 2(a)]. This state of interactions might continue at 298.15 K for PVP, but for BSA, this occurs at 298.15 and 313.15 K [Fig. 2(c)].

This linear trend at 298.15 K for PVP, due to its ketonic sites, and for BSA, due to its —COO^- and —N^+H_3 active sites, may interact strongly with water (shown later in Fig. 10), resulting in water monomer formation and destabilizing the water. This effect may further be enhanced as the temperature rises, and conformational changes may also occur in the PVP molecule.

The PVP monomer units are attached to vinyl C—C single bonds, and this could brighten the possibility for the rotation of PVP monomer units around C—C single bonds (shown later in Fig. 10), which results in conformational changes.[7] As for these changes, ρ for PVP does not vary uniformly with temperature. The BSA density in water at 283.15, 288.15, 303.15, and 308.15 K follows a polynomial trend. Although there is a linear variation at 293.15, 298.15, and 313.15 K, it decreases with concentration [Fig. 2(b)] at 313.15 K. This may happen because of the disruption of the BSA molecule.[8] The behavior of PVP in 0.01% BSA and water is visibly different from its behavior in water. The PVP solution density in BSA and water varies

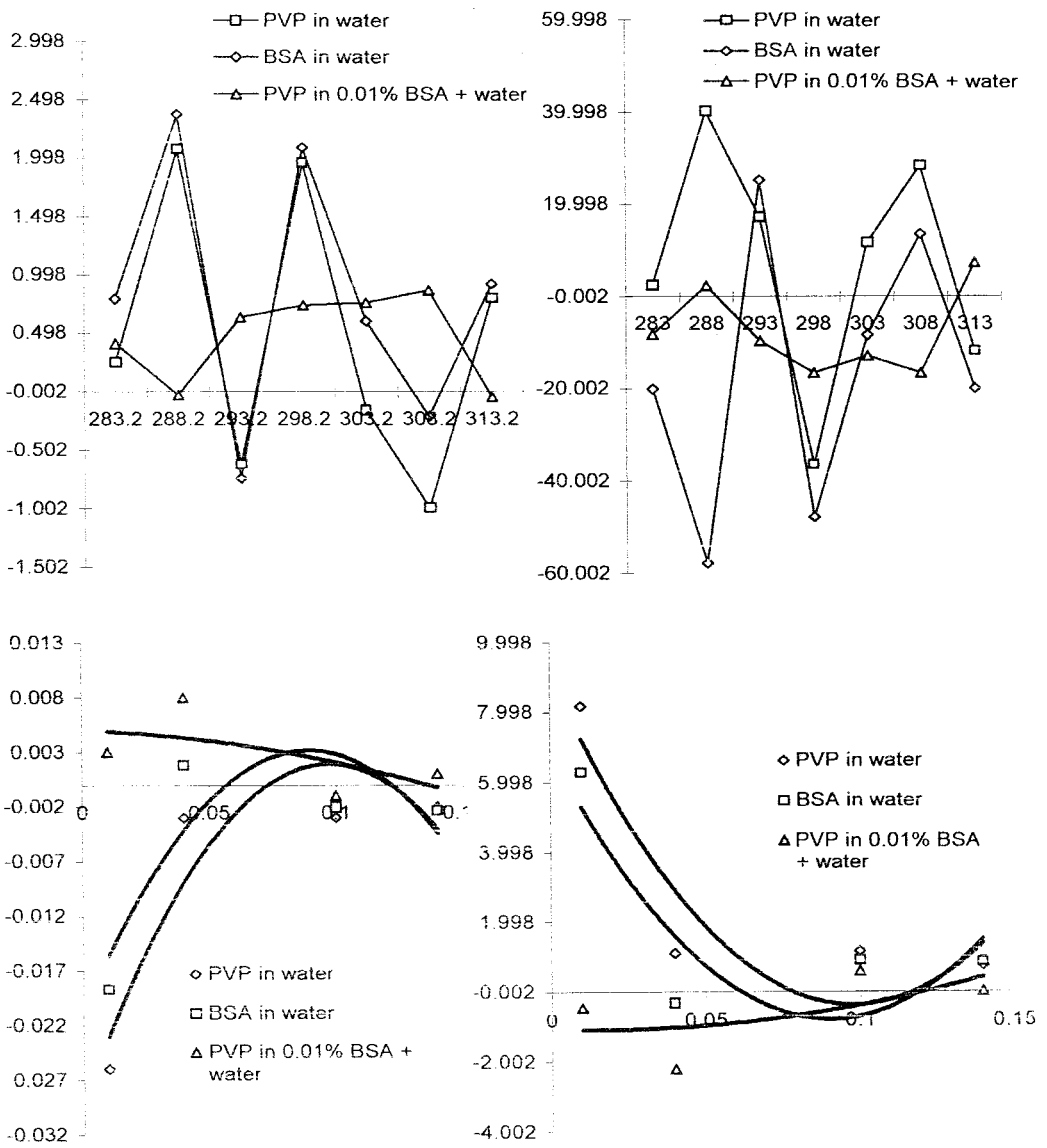

Figure 7 *B* (*y* axis) on the left and *D* (*y* axis) on the right versus the temperature (K; *x* axis) at the top and versus the concentration of the solute (*x* axis) on the bottom.

linearly with its concentration [Fig. 2(c)]. The addition of BSA (molecular weight = 65,000), which has a twisted helical shape, seems to exert a restriction on the free rotation of the PVP molecule and could later cause interactions with BSA. This may be because the different molecular portions of PVP molecules do not undergo conformational changes in the presence of BSA around a C—C single bond.

The dynamic viscosity decreases at each temperature and varies linearly with the concentration (Fig. 3). Notably, the difference in limiting viscosities ($\Delta\eta_0$) at consecutive temperatures decreases at higher temperatures, and so η_0 decreases as the temperature rises (Fig. 3 and Table IV). The PVP solution viscosity decreases with the addition of BSA. This can be attributed, perhaps, to the hydrophilic and hydrophobic interactions[7] of the hydrocarbon helical chain, —COO^- and N^+H_3 of BSA, and the vinyl chain and ketonic group of PVP molecules. The E^* value for the viscous flow of macromolecules in solution through a capillary (shown later in Fig. 8) increases with the PVP and BSA concentrations to some extent; after a certain concentration, E^* begins to decrease, and it intersects at a common point on the concentration axis. This could be seen in the common behavior of PVP and BSA in water. As shown in Figure 8 (shown later), E^* of PVP in water and 0.01% BSA varies linearly with a negative slope as the concentration increases. This concentration could be termed the critical concentration for the polymer molecules.

There is a specific trend for η_{red} for the chosen systems at the studied temperatures (Fig. 4), as their *B*

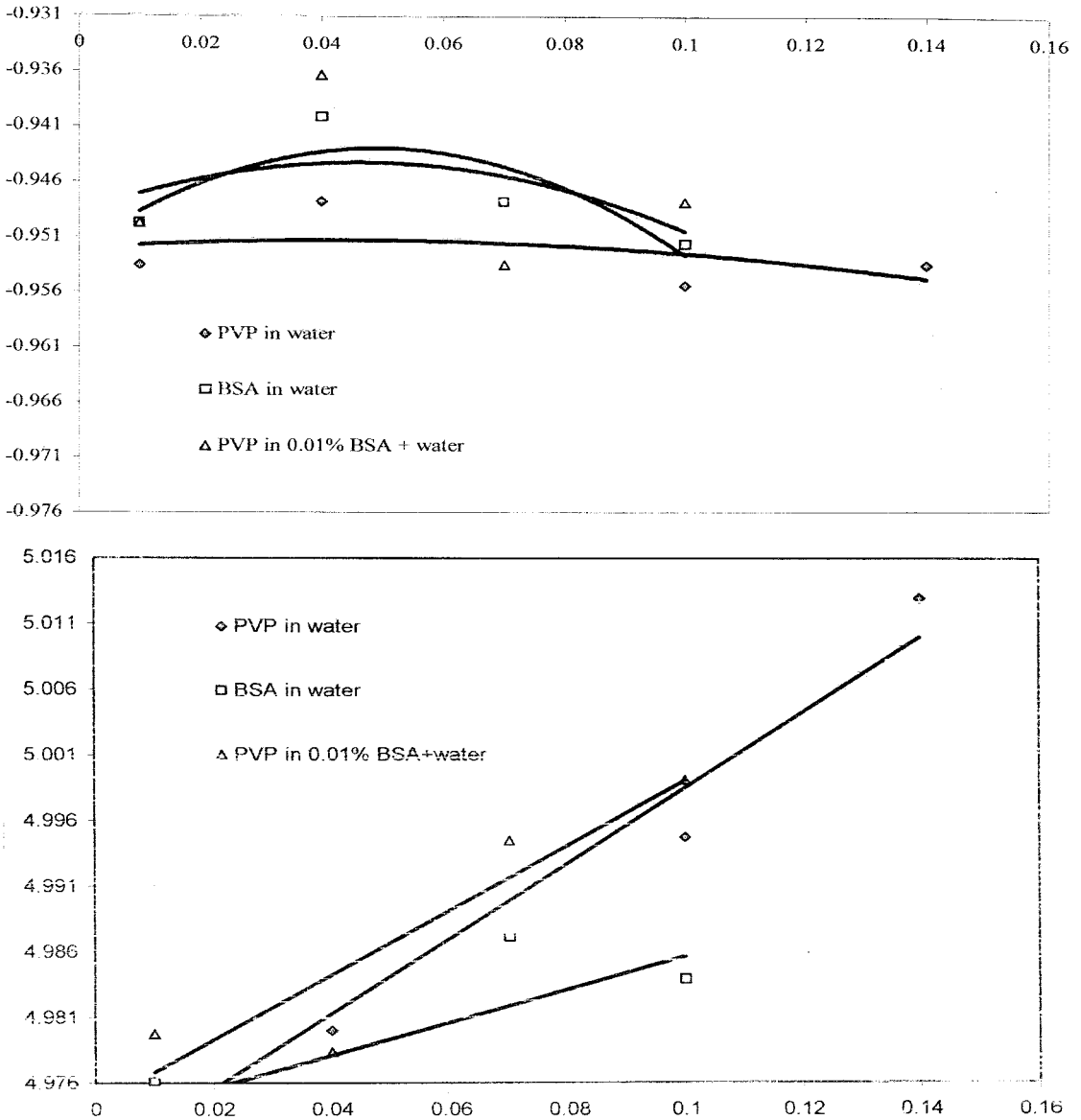

Figure 8 E^* of the viscous flow (J mol^{-1} K^{-1}; y axis) versus the solute concentration (wt %; x axis) at the top and the probability of the frequency factor or constant A (J mol^{-1} K^{-1}; y axis) versus the solute concentration (wt %; x axis) on the bottom.

values are maximum at infinite dilution and the same in general, approaching a common point with the lowest value. For PVP in water, the highest value of B is at 288.15 K, and the lowest is at 308.15 K, whereas for BSA in water, the highest is at 288.15 K, and the lowest is at 293.15 K, and for PVP in water and BSA, the highest is at 308.15 K, and the lowest is at 313.15 K (Fig. 4 and Table VI). This trend seems to match the $\lambda/4$ behavior, and in the same reference, one more overtone can be observed for PVP in water (Fig. 4) up to 0.14% PVP.

This trend further supports stronger PVP interactions with water at lower concentrations and temperatures, as shown in Figure 4.

The trends in η_{red}–temperature plots are similar for the chosen systems under the selected conditions, but PVP η_{red} values are lower at 303.15 K. This trend is different for BSA in water and for PVP in water and BSA (Fig. 5) and could be attributed to the increased rotation in the molecule and the hydrogen bonds breaking among the water molecules, water–PVP, water–BSA, and PVP–BSA–water.

Furthermore, interesting comparisons can be made of the values of PVP and BSA in water and of PVP in water and BSA (Fig. 6); in this case, there are intersecting nodes, with double nodes at 283.15 K for 0.05% BSA/PVP and water and for 0.11% BSA/PVP and water. Double nodes exist at 288.15, 298.15, 303.15,

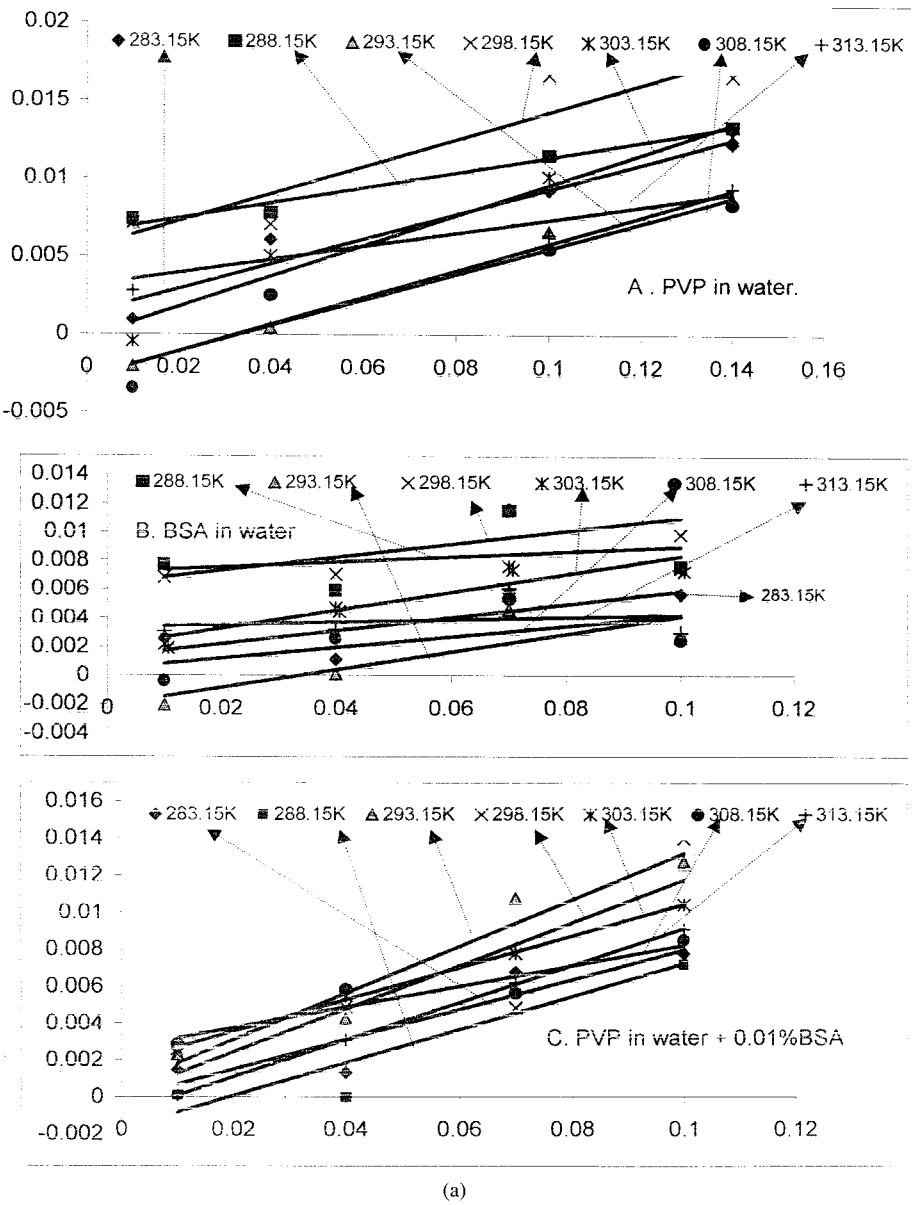

Figure 9 (a) v/V (y axis) versus the concentration (wt %; x axis) and (b) v/V (y axis) versus the temperature (K; x axis): (A,D) PVP in water, (B,E) BSA in water, and (C,F) PVP in water and 0.01% BSA.

308.15, and 313.15 K for similar systems. The nodes are shifted on the x axis, and they tend to shift to lower PVP concentrations. This behavior further supports more interactions at lower concentrations and temperatures for macromolecules of PVP and BSA (Fig. 6).

The B values for PVP and BSA in water are positive at 283.15, 288.15, 298.15, and 313.15 K. However, for PVP in water and BSA, the same are negative at 288.15 and 313.15 K (Fig. 7 and Table VI) and are maximum at 288.15 and 298.15 K. The B values for similar systems decrease rapidly as the temperature rises from 288.15 to 293.15 K and from 298.15 to 308.15 K (Fig. 7 and Table VI). The reverse trend of B is observed for D values for all chosen systems. The B and D values converge to a common point with increasing PVP concentration (Fig. 7). The B coefficient varies linearly for PVP in water and BSA as the temperature rises from 293.15 to 308.15 K; after this, it decreases. This shows that the original configuration of PVP disappears in the presence of BSA because of their intermolecular interactions. A reasonable interpretation may be assigned to the PVP coils, as they could expand because of the strong PVP–water and BSA–water interactions. As a result, the PVP molecular excluded volume in solution tends to increase.[9] Therefore, η_{red} decreases more rapidly as the concentration increases

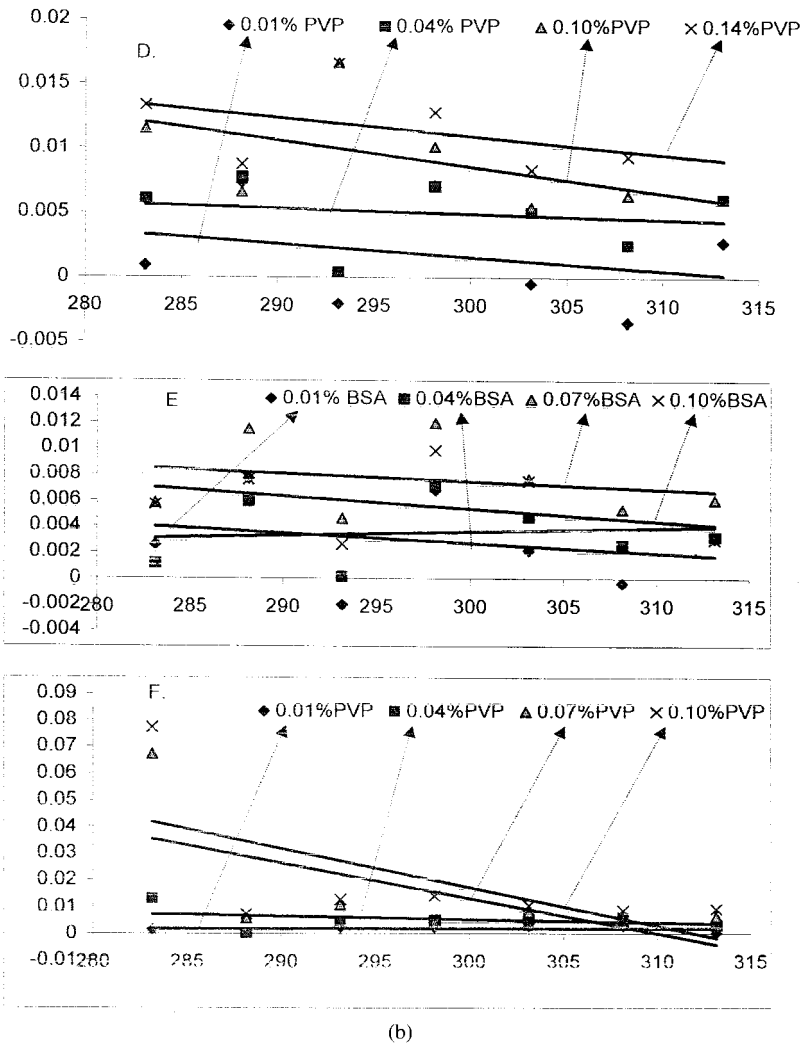

(b)

Figure 9 (*Continues from the previous page*)

at these temperatures (Fig. 6; 288.15, 298.15, and 313.15 K). The decrease in B and the increase in D are probably due to the decrease in PVP–BSA–water interactions[10–16] and the increase in PVP–PVP and PVP–BSA interactions, respectively.

Shape factor (v/V)

E^* for viscous flow for BSA in water and for PVP in water and BSA increases with concentration and reaches a maximum value at 0.06%; after that, it starts to decrease (Fig. 8). However, for PVP in water, it shows a linear trend with a negative slope with the PVP concentration:

$$(\eta - \eta^0)/\eta^0 = 5/2 \times v/V \qquad (8)$$

The mathematical solvent effect is nullified by $(\eta - \eta^0)/\eta^0$ as eq. (8) to determine the mathematical variations of PVP and BSA in water and of PVP in water and BSA. Because in eq. (8) V is constant (the bulb capacity is fixed), the water viscosity is constant, and so for such a mathematical state, the viscosity variation of the chosen systems is directly related to their molecular shape and size. v (the single molecule volume) varies linearly with the concentration with a positive slope [Fig. 9(a)] and with visible deviations [Fig. 9(b)]. The deviations could be due to the localized thermal vibrations around active sites of PVP and BSA molecules. However, the thermal vibrations seem insufficient to compete with the PVP and BSA molecular integrating forces. The trend is supported by the linear behavior of PVP in water and in water and BSA [Fig. 9(a,b)]. This linearity could be the function of their increasing concentration. Had there been any molecular breakage due to thermal vibrations, the linearity behavior would have been abrupt. Therefore, we have explored the nonbreakable behavior of PVP and BSA in water and of PVP in water and BSA.

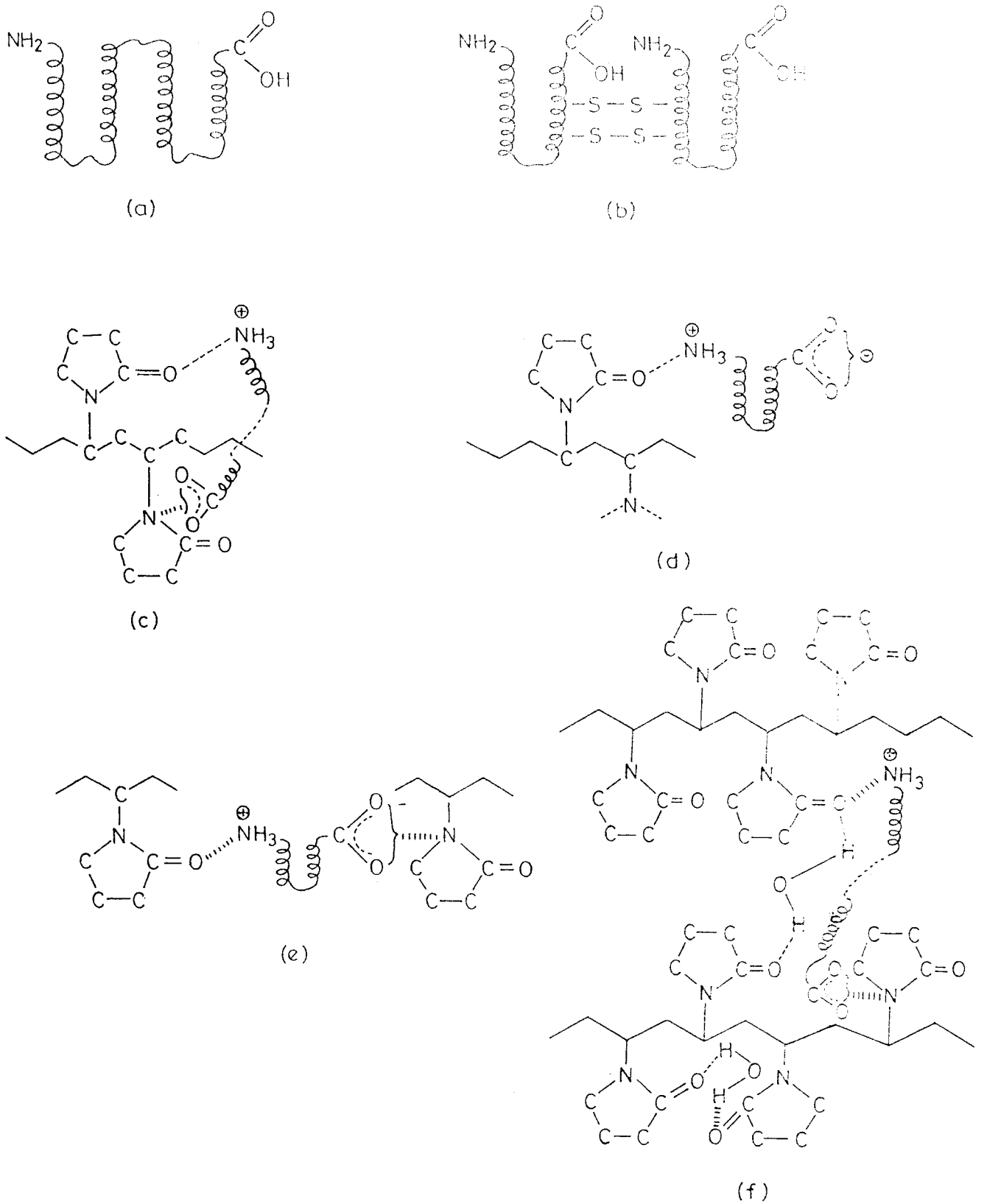

Figure 10 (a) (b) Coil of BSA. (c) (d) (f) Shows interactions between active sites of PVP and BSA.

A comparatively increased solution temperature inhibits hydrogen-bond formation on active sites of PVP and BSA in water (Fig. 10). The addition of BSA further enhances this effect [Fig. 9(a-C,b-F)]. From the bottom to the top along the y axis, the shape factor seems to be a function of the concentration, leading to PVP (water) hydrated cospheres. The hydrophobic backbone of PVP may induce hydrophobic interactions (Fig. 10). Similarly, from left to right along the x axis [Fig. 9(b-F)], it seems to be a function of temperature. Perhaps the shape factor could stabilize at a particular temperature point [Fig. 9(b-F); 308.15 K].

Under our chosen conditions, polymer molecules flowing through a capillary of the viscometer face the rigid capillary cubical boundary with the quantum behavior of a particle:[17]

$$\frac{\partial^2\psi}{\partial x^2} + \frac{\partial^2\psi}{\partial y^2} + \frac{\partial^2\psi}{\partial z^2} + \frac{8\pi^2 m}{h^2} - E\psi = 0 \qquad (9)$$

Equation 9 extracts nonbreaking (rigid) molecular reversible flow motions with E and a ψ position function (x, y, z). The molecules, when the flow begins from the viscometer (with a 5-cc bulb), resemble the zero state of energy:

$$E = n\left(\frac{h^2}{8\pi^2 I}\right) \qquad (10)$$

where n is the number of rotational motions of PVP and BSA. I is the reduced mass of PVP and hydrated water molecules. As in the bulb, the molecules are in a resting position before the flow with thermal and position equilibrium, as the experimental conditions do not vary; the flow of PVP and BSA molecules is exposed (as Schrodinger boundary wall conditions are fixed) to the new boundary conditions (capillary) under chosen experimental conditions. The linearity trend [Fig. 9(a,b)] for the shape factor with an increased number of PVP particles (increased concentration) and increased energy (thermal) could simply predict the parameters of the shifted equilibrium condition to a higher state within a similar constitutional framework. The Schrodinger quantum equation is a demand and can be treated as the new genesis or composition for a remarkable approach explaining the shape factors of PVP and BSA in water and of macromolecules in solution in general.[15] This extraction, supported by our data, provides conclusive evidence that under our variables (concentration and temperature), the shape of the polymer is functional, determining the physicochemical behavior of PVP and BSA in aqueous solutions. The same can be extended to macromolecules of a similar nature or constitution, for which the viscosity, zero-state energy equation, and general Schrodinger equation become fundamental for such information.

References

1. Papanagopoulos, D.; Dondos, A. Polymer 1996, 37, 1053.
2. Tewari, N.; Srivastav, A. K. Macromolecules 1992, 25, 1053.
3. Danait, A.; Deshpande, D. D. Eur Polym J 1995, 31, 1221.
4. Inai, Y.; Takenouchi, S.; Hirabayashi, T.; Yokota, K. Polym J 1996, 28, 365.
5. Yang, H.; Zhu, P.; Li, G.; Wu, P.; Ren, F. Eur Polym J 1999, 35, 365.
6. Elvers, B.; Hawkins, St.; Schulz, G. Ullman's Encyclopedia of Industrial Chemistry; VCH Publishers: New York; Vol. A21, p 753.
7. Nakano, A.; Minoura, Y. J Appl Polym Sci 1977, 21, 2877.
8. Jirgensons, B.; Mark, H. F; Gaylord, N. G.; Bikales, N. M., Eds. Encyclopedia of Polymer Science and Technology; Interscience Publishers: New York, London, Sydney; Vol. 1, p 575.
9. Yang, H.; Zhu, P.; Xie, Y.; Zhang, X.; Li, G. Polymer 2000, 41, 499.
10. Wu, C. J Polym Sci Part B: Polym Phys 1994, 32, 1503.
11. Liu, M.; Cheng, R.; Qian, R. J Polym Sci Part B: Polym Phys 1995, 33, 1731.
12. Dondos, A.; Tsitsilianis, C. Polym Int 1992, 28, 151.
13. Montelro, E. E. C.; Thaumaturgo, C. Polym Bull 1993, 30, 697.
14. Papanagopoulos, D.; Dondos, A. Macromol Chem Phys 1994, 195, 439.
15. Dondos, A.; Papanagopoulos, D. Polymer 1995, 36, 365.
16. Zhu, P. W. Eur Polym J 1995, 31, 659.
17. Donald, A.; McQuarrie. Quantum Chemistry; University Science Books California, Oxford University Press: Oxford, 1983; p 69.
18. Levitt, B. P. Findley's Practical Physical Chemistry, 9th ed.; Longman Inc: New York, 1973.